This is a preprint, the final version is subject to change, of the American Mineralogist (MSA)
Cite as Authors (Year) Title. American Mineralogist, in press.
(DOI will not work until issue is live.) DOI: http://dx.doi.org/10.2138/am-2017-5898

Revision 1

Barometric constraints based on apatite inclusions in garnet

Kyle T. Ashley[1,*], Drew W. Barkoff[2], and Matthew Steele-MacInnis[2]

[1] Department of Geologic Sciences, Jackson School of Geosciences, University of Texas at Austin, 2275 Speedway Stop C9000, Austin, TX 78712, USA

[2] Department of Geosciences, The University of Arizona, 1040 E. 4th Street, Tucson, AZ 85721, USA

[*]*Corresponding author: Tel. +1 315 244 5546; E-mail: ktashley@utexas.edu*

Running title: Apatite-in-garnet barometry

This is a preprint, the final version is subject to change, of the American Mineralogist (MSA)
Cite as Authors (Year) Title. American Mineralogist, in press.
(DOI will not work until issue is live.) DOI: http://dx.doi.org/10.2138/am-2017-5898

Barometric constraints based on apatite inclusions in garnet

ABSTRACT

Compiled volumetric data for fluor-, chlor- and hydroxyl-apatite has been fitted to a pressure-volume-temperature (*P*-*V*-*T*) equation of state for volume calculation at elevated *P* and *T*. The regressions were used to assess the potential of apatite inclusions in garnet for thermobarometric applications, according to the pressurization of inclusions resulting from elastic differences between the inclusion and host minerals. Isomeke contours (lines in pressure temperature space, representing permissible entrapment conditions that yield a given inclusion pressure) were calculated and show that apatite inclusions in garnet are a particularly useful barometer, owing to the large differences in the bulk moduli and similar thermal expansivities between apatite and garnet. Heating experiments were conducted on fluorapatite inclusions in andraditic garnets from the Casting Copper skarn, NV, to assess the variation in measured inclusion pressure with heating relative to that predicted with isotropic elastic theory. Negligible departures between theoretical and measured pressurization suggests no significant correction is needed for applying room-*T* inclusion pressure measurements for barometry constraints.

Keywords: apatite, garnet, pressure, heating, Raman spectroscopy

INTRODUCTION

Apatite is the most abundant phosphate mineral on Earth and commonly occurs as an accessory phase in igneous and metamorphic rocks, and as detritus in sedimentary rocks. The chemistry of Ca-apatite is $Ca_5(PO_4)_3X$, where X is occupied by a halogen element or volatile compound, with the major endmembers being fluorapatite (FAP), chlorapatite (CAP) and hydroxyapatite (HAP), in which X= F, Cl and OH, respectively. Pure FAP and HAP have been experimentally shown to be stable at pressures up to 11–13 GPa at 1300–1800 K before decomposing to a $Ca_3(PO_4)_2$ pseudomorph (Murayama et al. 1986), and apatite is stable to at least 7.5 GPa at 950 °C when a component in mid-ocean ridge basalts (Konzett and Frost 2009). Thus, apatite is stable at conditions from Earth's surface through the upper mantle. The ubiquitous occurrence of apatite as an accessory phase in a wide variety of rock types and across large ranges of pressure (P) and temperature (T) makes apatite an attractive mineral for petrologic applications such as interpreting pressure-temperature-time paths. Here, we describe application of apatite in thermobarometry, according to the physical properties of apatite inclusions in garnet.

The growth of minerals in rocks may result in the encapsulation of crystallites (either preexisting mineral grains, or mineral grains produced via metamorphic reactions) within larger mineral grains. At the time of entrapment, the molar volumes of the host and inclusion minerals correspond exactly to the same P-T conditions of encapsulation. However, upon exhumation, any elastic difference between the host and inclusion may lead to the pressurization of the inclusion mineral, such that at Earth's surface inclusion pressure (P_{incl}) differs from the externally applied pressure (1 bar). Garnet commonly occurs as poikiloblasts in metamorphic rocks, in which inclusions of quartz, calcite, micas, feldspars, and accessory phases are commonly reported.

Analysis of inclusions in garnet has been used for numerous purposes, including: bracketing the timing of garnet growth (Catlos et al. 2001), correlating garnet growth to deformation and fabric development (e.g., Passchier and Trouw 2005, and references therein), reconstructing conditions of early-prograde deformation (Ashley et al. *accepted*), constraining fluid flux and composition (e.g., Vry and Brown 1991), and barometry from pressurized quartz inclusions (e.g., Rosenfeld and Chase 1961; Enami et al. 2007; Ashley et al. 2014).

Garnet is a suitable host mineral for thermobarometry of mineral inclusions because it is an isotropic host with a high bulk modulus. The high bulk modulus of garnet allows for stress retention within the inclusions, leading to the development and preservation of inclusion pressure upon exhumation. Previous studies of mineral inclusions have focused mainly on thermobarometry based on inclusions of silica polymorphs within garnet (namely quartz and coesite). However, similar to quartz, apatite is a relatively soft, compressible mineral that would be expected to develop pressurization if entrapped at elevated pressures and exhumed to Earth's surface. As noted above, apatite is a common accessory phase and is a typical inclusion phase within garnet in some environments. Moreover, apatite is characterized by a sharp, easily resolvable Raman band at ca. 964 cm^{-1}, and experimental data for the pressure-dependent shift of this Raman band are available (e.g., Comodi et al. 2001; Schouwink et al. 2010). In this paper, we present new modeling of the physical and spectroscopic characteristics of apatite for applications in thermobarometry. This modeling indicates that apatite inclusions in garnet represent a robust barometer. To test this approach, fluorapatite inclusions and andradite garnet from the Casting Copper skarn, NV, are measured for a range of temperatures (-175 to 275 °C) to internally test the ability of the modeling approach to replicate inclusion pressure variations with heating and cooling.

METHODS

Parameterization of the elastic properties of apatite endmembers

Experimental data on the unit-cell volume of apatite were fitted to a pressure-volume-temperature equation of state (*P-V-T* EOS) to permit calculation of volumes at any *P* and *T* condition of interest. We used the modified 3rd-order Tait EOS of Holland and Powell (2011), which applies a thermal pressure formulation to correct for volume expansion at elevated temperature. The volumetric data was compiled from the sources listed in Table 1. EOS regressions were completed using the program *EosFit7-GUI* (Gonzalez-Platas et al. 2016) assuming hexagonal symmetry (Hughes et al. 1989), which applies the refinement methodology after Angel et al. (2014). Estimated standard deviations (ESDs) in elastic moduli were calculated through a least-squares fitting approach using the pressure, temperature and volume standard deviations reported in the experimental literature (Table 1). An estimated Einstein temperature (θ_E) was calculated following the protocol of Holland and Powell (2011), using the standard entropy at 298 K ($\boldsymbol{S}°_{298}$) and 21 atoms per unit formula for apatite; the quality of θ_E estimation was evaluated by ensuring minimized ESDs occurred at the value calculated and that significant improvements were not made on the refinements when the temperature was varied. The calculated elastic moduli are listed in Table 2, with a comparison of modeled and experimental molar volumes shown in Figure 1. Volumes of garnet at elevated *P* and *T* were calculated using the thermochemical database of Holland and Powell (2011, and references therein).

Elastic theory and modeling encapsulation pressures

Entrapment pressure was calculated for a given inclusion pressure (P_{incl}) by applying the 1D isotropic elastic model of Guiraud and Powell (2006):

$$\left(\frac{V_{1,298}}{V_0}\right)_{host} = \left(\frac{V_{incl,298}}{V_0}\right)_{incl} - \frac{3}{4G} \cdot (P_{incl} - P_{ext}) \quad \text{eq. 1}$$

where V_0 is volume at the conditions of entrapment, $V_{P,298}$ is volume at Earth's surface (P of 1 bar for garnet and P_{incl} for the inclusion), G is the shear modulus of the host, and P_{ext} is the externally applied pressure at the time of measurement (1 bar). The procedure for computing entrapment pressure at a given temperature is as follows: For a known (measured) P_{incl} and a known or inferred entrapment T, the value of the entrapment pressure is adjusted iteratively and the V_0's of the inclusion and host are computed at each pressure value. Entrapment pressure is determined when both sides of eq. 1 are equal. The "isomeke" (Adams et al. 1975) of a given P_{incl} corresponds to the locus to temperature-entrapment pressure points that satisfy eq. 1. As such, to construct the isomeke, the procedure described above is repeated for a range of entrapment T's to determine the corresponding entrapment pressures. In this study, an isomeke contour map was generated for each apatite endmember included in garnet, $X_3Y_2(SiO_4)_3$ (Fig. 2). The garnet endmembers included here include almandine, pyrope and andradite. Almandine and pyrope represent maximum and minimum entrapment pressure estimates, respectively, for garnet endmembers with the Y-site occupied by Al and the X-site occupied by Fe, Mn, Mg and Ca. Andradite, $Ca_3Fe_2(SiO_4)_3$, is a common garnet species in hydrothermal skarn deposits, and is characterized by elastic moduli significantly different from those of other modeled garnets. The shear moduli for almandine, pyrope and andradite are 921, 902 and 860 kbar, respectively (Wang and Ji, 2001). Although not included in Fig. 2, isomekes for other garnet endmembers (e.g.,

122 spessartine, grossular) can be estimated based on those for the calculated (extreme) end-
123 members, according to the relative magnitudes of their compressibilities, expansivities and shear
124 moduli. For example, isomekes for grossular (shear modulus ca. 98.1 GPa) would fall between
125 those projected for apatite in almandine (Fig. 2a-c) and pyrope (Fig. 2d-f), and would be <1 kbar
126 offset from either of these latter two endmembers
127

128 **Raman spectroscopy and heating experiments**

129 Samples analyzed in this study included fluorapatite from Durango, Mexico, and
130 fluorapatite inclusions within andradite garnet from Casting Copper, Nevada. The Durango
131 apatite sample was a single crystal, which was cut into a ca. 500 μm-thick wafer and doubly
132 polished. The Casting Copper apatite grains are μm-sized inclusions within euhedral garnet
133 grains. The garnet grains were cut into ~1000 μm-thick wafers and doubly polished. Apatite
134 inclusions within the garnet grains were then identified using transmitted light microscopy.
135 Polishing of the garnet samples also resulted in some apatite inclusions being exposed on the
136 polished surface of the garnet wafer, and these exposed inclusions were identified using reflected
137 light microscopy.
138 Unpolarized Raman spectra were collected using a Thermo Nikolet Almega microRaman
139 system at the Mike Scott Laboratory for Mineralogy and Crystallography at the University of
140 Arizona. Raman spectra were collected in a back-scattering arrangement. We used a 532 nm
141 excitation laser, with laser power set to ~100 mW. Focusing of the excitation laser onto the
142 polished apatite wafer (Durango) and the apatite inclusions within garnet grains (Casting
143 Copper) was accomplished using a Nikon 10x, long working distance objective on an Olympus

144 BX51 microscope. The spectrometer position was calibrated using the ca. 1100 cm^{-1} Raman line
145 of sparry calcite.

146 For the heating and cooling experiments, we used a Linkam THMSG600 stage mounted
147 on the Raman microprobe. Temperature settings of the stage were calibrated using synthetic
148 fluid-inclusion standards (triple point of CO_2 at -56.6 °C; triple point of H_2O at 0.01 °C; critical
149 point of H_2O at 374.1 °C), and is accurate to within ±0.1 °C from subzero temperatures to ~100
150 °C, and to within ±0.5 °C at higher temperatures. Temperature-dependent Raman measurements
151 (Fig. 3) were conducted at 50 °C increments from 25 to +275°C, and each measurement was
152 replicated also on the cooling path from 275 to 25 °C to confirm that the inclusions had not been
153 modified by plastic deformation. Subsequently, the samples were also analyzed along a cooling
154 path at 50 °C increments from 25 to -175 °C, with replicate analyses conducted along the
155 associated re-heating path to room temperature. At each temperature (from -175 to 275 °C), we
156 analyzed the wafer of the Durango apatite standard, and several inclusions at or below the
157 surface of the Casting Copper garnet wafers. The calcite standard was analyzed before and after
158 each temperature profile to check and potentially correct for spectrometer drift (no drift was
159 detected).

160 Raman spectra were analyzed using the software package PeakFit v.4.11 from SYSTAT
161 Software Inc. The workflow involved a linear baseline subtraction followed by peak fitting using
162 a Gaussian+Lorentzian Area model. Satisfactory fitting of the apatite ν_{964} peak (i.e., the
163 phosphate symmetric stretch, $\nu_1(A_g+E_{2g})$ mode; Comodi et al., 2001) was accomplished by using
164 three peaks: the main sharp peak centered at ca. 964 cm^{-1}, and two broader, shorter peaks
165 centered at ca. 950 and 1030 cm^{-1}. The latter of these peaks corresponds to the asymmetric
166 stretch, $\nu_{3b}(E_{2g})$ vibrational mode of phosphate, according to Comodi et al. (2001). The peak

centered at ca. 950 cm^{-1} is manifested only as a slight, lower-wavenumber shoulder on the larger ν_{964} peak; according to Liu et al. (2008), this shoulder represents a distortion of the symmetric stretching mode owing to radiation damage (fission tracks) in apatite. Our estimated uncertainty on peak position is approximately ±0.141 cm^{-1}, according to replicate measurements and peak fitting performed on the Durango apatite standard during every analytical session.

The methods for defining the pressure- and temperature-dependent Raman waveshifts of minerals is described in detail by Watenphul and Schmidt (2012). Briefly, the shift in Raman peak position with respect to that at a reference temperature and pressure (normally, 25 °C and 1 bar) is expressed as:

$$\Delta\boldsymbol{\nu_i}(\boldsymbol{P},\boldsymbol{T}) = \boldsymbol{\nu_i}(\boldsymbol{P},\boldsymbol{T}) - \boldsymbol{\nu_i}\left(\boldsymbol{P_{ref}},\boldsymbol{T_{ref}}\right)$$

$$= (\Delta\boldsymbol{\nu_i})_{\boldsymbol{P},\boldsymbol{T_{ref}}} + (\Delta\boldsymbol{\nu_i})_{\boldsymbol{T},\boldsymbol{P_{ref}}} + (\Delta\boldsymbol{\nu_i})_{\boldsymbol{P},\boldsymbol{T}} \qquad \text{eq. 2}$$

where $(\Delta\boldsymbol{\nu_i})_{\boldsymbol{P},\boldsymbol{T_{ref}}}$ is the pressure-dependent contribution at the reference temperature, $(\Delta\boldsymbol{\nu_i})_{\boldsymbol{T},\boldsymbol{P_{ref}}}$ is the temperature-dependent contribution at the reference pressure, and $(\Delta\boldsymbol{\nu_i})_{\boldsymbol{P},\boldsymbol{T}}$ is the remaining contribution referred to by Watenphul and Schmidt (2012) as the "cross term." The latter term reflects any variation in the temperature dependence with changing pressure or the pressure dependence with changing temperature. For several minerals, available experimental data indicate that the cross term is negligible and can be assumed to be zero (e.g., quartz: Schmidt and Ziemann, 2000; fully crystalline zircon: Schmidt et al., 2013). However, this assumption must be tested on a case-by-case basis for other minerals.

Inclusion pressures for fluorapatite inclusions at room temperature can be determined through the *P*-sensitive frequency shift of the 964 cm^{-1} band or by *in situ* X-ray diffraction (Fig.

4). The polynomial for the $\boldsymbol{P - \Delta\nu_{964}}$ relationship at 25 °C, calculated with the experimental data of Schouwick et al. (2010), is

$$\boldsymbol{P\ (\mathrm{bar}) = \left(a \cdot (\Delta\nu_{964})^2_{P,T_{ref}}\right) + \left(b \cdot (\Delta\nu_{964})_{P,T_{ref}}\right)} \quad \text{eq. 3}$$

where *a* and *b* are regression parameters equal to 7.35 ± 1.88 and 2265 ± 59, respectively. The results obtained using this expression are very similar to pressures calculated using the equation of Comodi et al. (2001). The parameter $(\Delta\nu_{964})_{P,T_{ref}}$ represents the difference between the measured peak position and the reference (1 bar) peak position, at the reference temperature of 25 °C.

RESULTS

The data shown in Fig. 5 allow us to define the temperature-dependent portion of eq. 2. For this regression analysis, we included both the temperature-dependent waveshift of the Durango fluorapatite standard, as well as the temperature-dependent waveshift of a Casting Copper apatite inclusion that was exposed to the sample surface during polishing. Thus, all data shown in Fig. 5 correspond to a reference pressure of 1 bar. The polynomial expression derived from regression analysis of these data is:

$$\boldsymbol{(\Delta\nu_{964})_{T,P_{ref}}\ (\mathrm{cm^{-1}}) = c \cdot T^2 + d \cdot T + e} \quad \text{eq. 4}$$

where *T* is in °C and *c, d* and *e* are regression coefficients equal to -0.0000134 ± 0.0000011, -0.0070 ± 0.00018, and 0.287 ± 0.029, respectively (Fig. 4). The parameter $(\Delta\nu_{964})_{T,P_{ref}}$

213 represents the temperature-dependent waveshift, relative to 25 °C, at the reference pressure of 1
214 bar. Combining equations 2, 3 and 4 (Watenphul and Schmidt, 2012) yields the general
215 expression:
216
217 $$\boldsymbol{P}\,(\mathbf{bar}) = \boldsymbol{a}\cdot(\Delta\boldsymbol{\nu_{964}} - \boldsymbol{c}\cdot\boldsymbol{T^2} - \boldsymbol{d}\cdot\boldsymbol{T} - \boldsymbol{e})^2 + \boldsymbol{b}\cdot(\Delta\boldsymbol{\nu_{964}} - \boldsymbol{c}\cdot\boldsymbol{T^2} - \boldsymbol{d}\cdot\boldsymbol{T} - \boldsymbol{e}) \qquad \text{eq. 5}$$
218
219 Equation 5 represents the combined temperature- and pressure-dependent Raman shift,
220 and can thus be used to compute inclusion pressures from -175 to 275 °C. Coefficients a-e are
221 the same as those listed for eqs. 3 and 4 (above). Notice that eq. 5 assumes a negligible cross
222 term, analogous to the study by Watenphul and Schmidt (2012), although validation of this
223 assumption for apatite will require future experiments.
224 Pressures of fully encapsulated apatite inclusions from Casting Copper were calculated
225 using eq. 5, with the reference peak position ($\boldsymbol{\nu_{964}}$) determined based on the measurements of
226 the inclusion exposed to the sample surface (Table 3). The Durango apatite standard was not
227 used for the reference peak position because we noted systematic differences between the 1 bar
228 peak positions of Durango standard versus the exposed apatite inclusions from Casting Copper
229 (Table 3). These differences are thought to reflect chemical effects according to substitutions in
230 the X (halogen) site in the apatite structure. Specifically, apatite from Durango contains
231 approximately ~3.5 wt% F and 0.4 wt% Cl on average (Young et al., 1969) whereas apatite
232 inclusions from Casting Copper contain on average 2.7 wt% F and 0.1 wt% Cl (D. Barkoff,
233 *unpublished data*), with more significant mixing between the F and OH endmembers. Thus,
234 standardizing the inclusion measurements according to an exposed inclusion on the sample

surface seems to be the best practice, implicitly accounting for the chemical composition of the apatite inclusions in a given sample.

The fully encapsulated inclusions of apatite in garnet from Casting Copper exhibit negative waveshifts at 25 °C, indicating that the inclusions are under tension at ambient temperature. Similar phenomena have been reported for quartz inclusions in garnet from relatively high-temperature, low-pressure terranes (e.g., Kouketsu et al. 2014; Ashley et al., 2015). During heating to 275 °C, the fully encapsulated inclusions undergo progressive pressurization (Table 3, Fig. 6), owing to the differential thermal expansion of inclusion and host. Conversely, cooling the sample to subzero temperatures results in decreased pressure within the inclusions (i.e., increased tensile stress). The pressure variations within the inclusions induced by both heating and cooling appear to be elastic and reversible in nature, as indicated by the replicate analyses conducted during re-cooling/re-heating the sample to room temperature (Table 3).

DISCUSSION

Temperature and Pressure sensitivity of the ν_{964} band of apatite

Equations 4 and 5 allow us to assess the temperature and pressure sensitivity of the $\boldsymbol{\nu_{964}}$ band of apatite, which are factors in evaluating the usefulness of apatite for barometry. From eq. 4, the average $\boldsymbol{\delta\upsilon/\delta P}$ slope of apatite is approximately ~4.4 cm^{-1}/GPa at 1 bar, increasing gradually with increasing pressure. For comparison, the average $\boldsymbol{\delta\upsilon/\delta P}$ slope of the ~464 cm^{-1} peak of quartz is 9 cm^{-1}/GPa (Schmidt and Ziemann 2000), and that of the ~1008 cm^{-1} peak of fully crystalline zircon is 5.7 cm^{-1}/GPa. As such, apatite is less suitable for spectroscopic barometry (i.e., has a lesser peak shift for equivalent pressurization) than these two latter

minerals, but nevertheless the apatite pressure is still resolvable and quantifiable by peak fitting. In terms of temperature sensitivity, the 464 cm^{-1} band of quartz exhibits a modest temperature sensitivity of only ~-0.014 cm^{-1}/°C (Schmidt and Ziemann 2000), making quartz well suited for pressure determination at elevated temperatures, for example in hydrothermal diamond-anvil cells (HDACs). Fully crystalline zircon shows a greater and more variable temperature sensitivity of the 1008 cm^{-1} peak position, from ~-0.03 cm^{-1}/°C at room temperature to ~-0.04 cm^{-1}/°C at $T \geq 500$ °C (Schmidt et al. 2013). Schmidt et al. (2013) noted that relative sensitivity of the zircon peak position to temperature implies that temperatures must be well known in order to use zircon as pressure sensor in HDACs. In comparison, apatite shows a relatively modest temperature sensitivity of the ca. 964 cm^{-1} peak position, more comparable to that of quartz: at room temperature, $\boldsymbol{\delta v/\delta T}$ of the apatite 964 cm^{-1} peak is just -0.008 cm^{-1}/°C, and at 300 °C $\boldsymbol{\delta v/\delta T}$ and the same peak is -0.015 cm^{-1}/°C. As such, apatite may be a fairly suitable spectroscopic pressure sensor for HDAC experiments. Certainly, quartz provides a better pressure sensitivity, but in some circumstances quartz becomes unsuitable for HDAC experiments because of high solubility in aqueous fluids (e.g., Schmidt et al. 2013) such that the quartz grain used for barometry may be partially or completely dissolved in the aqueous solution within the HDAC. In such cases, apatite may represent an alternative. For example, Antignano and Manning (2008) reported fluorapatite solubilities in H_2O that were in some cases approximately three orders of magnitude less than that of quartz at similar pressure-temperature conditions.

Applicability of apatite inclusions in garnet for barometry constraints

Figure 2 shows the significant dependence on entrapment pressure and not on entrapment temperature for the pressurization of apatite inclusions in garnet, indicating that apatite inclusions in garnet are suitable for barometric constraints. The slope of the contoured isomekes and the spacing between them can be explained by comparing the elastic moduli between the inclusions and hosts. Andradite, which has the greatest thermal expansivity of the modeled garnet species (2.86 x 10^{-5} K^{-1}; Holland and Powell, 2011) and thus that most similar to apatite (3.0–3.4 x 10^{-5} K^{-1}), exhibits the smallest thermal dependency (i.e., flatter isomeke slopes; Fig. 2). Andradite also has a lower bulk modulus compared to almandine and pyrope, resulting in less pressure sensitivity of the barometer (i.e., isomekes are spaced further apart). Chlorapatite has the lowest thermal expansivity and therefore the least thermal dependence for entrapment pressure constraint. Interestingly, chlorapatite inclusions in andradite transition from isomeke contours with a slight positive slope at low *P*, to no slope at ~6 kbar, to a negative slope at higher *P* (Fig. 2h). This latter phenomenon results from the thermal expansivity of andradite being greater than that of CAP at elevated *P*. However, caution should be used when using the fitted equation of state for CAP because the lack of high-quality *P*-*V* data resulted in the poorest quality of fit and the largest uncertainties on the elastic parameters among the three apatite endmembers (Table 2). Regardless, all apatites show good pressure sensitivity that makes any endmember suitable for barometric constraints. Mixing between FAP and HAP is expected to only introduce small changes to the calculated entrapment pressures as long as the dominant endmember isomeke contours are used. The isothermal bulk modulus of carbonated hydroxyapatite is significantly decreased by the presence of carbonate (up to ~20%; Liu et al. 2011; Forien et al. 2015). This lower bulk modulus is advantageous for barometry, resulting in improved pressure retention and sensitivity of the apatite-in-garnet barometer. Calorimetric

measurements made by Hovis and Harlov (2010) for mixing between the fluor- and chlorapatite species recognized a high degree of thermodynamic non-ideality (without any detected miscibility gap); therefore caution should be used when applying this technique to inclusions with significant mixing along the F-Cl join. We recommend using the fluorapatite projections whenever possible because fluorapatite is the most abundant endmember of apatite in rocks (Hovis et al. 2015), especially at higher temperatures where devolitization reduces the mole fraction of hydroxyapatite, and most of the single-crystal compression and heating experimental data has been reported for this endmember, allowing for improved EOS fitting.

Insights gained from *in situ* heating experiments on apatite inclusions within garnet

Heating experiments conducted on inclusions in garnet are important for two reasons. Firstly, the heating experiments can be used to confirm that the inclusions record residual pressures owing to elastic deformation. The difference between the Raman peak position of Durango apatite and the Casting Copper apatite exposed at the sample surface (described above) highlights a potential complexity in using apatite inclusions for barometry: Namely, that the Raman peak position is affected by the chemical composition of apatite. Quartz inclusions in garnet, which have been more commonly used in barometry, do not suffer from this complication owing to extremely limited solid solution in quartz. Apatite, by contrast, can accommodate an array of major and trace elements, and as such, the reference standard for computing $\Delta\nu_{964}$ should be closely matched to the targeted unknowns. The procedure described herein, using one or more apatite inclusions exposed to the surface *of the same garnet crystal* as reference, provides an obvious method to ensure close matching of reference and unknown. However, the

possibility of a single garnet grain hosting apatite grains of different compositions cannot be excluded a priori. Therefore, heating experiments provide a method to test that the Raman shift exhibited by encapulated inclusions records a reproducible inclusion pressure. For example, the inclusions shown in Fig. 6 show pressurization with increasing temperature, and a return to tensile conditions upon subsequent cooling – neither of which would occur as a result of chemical differences between inclusion and reference material. Thus the heating experiments provide confidence that the inclusions are not compromised.

The second reason that heating experiments on mineral inclusions are useful is for testing the quality of the modeling approach when calculating entrapment pressures. For quartz inclusions in garnet, a significant offset between modeled and measured P_{incl} with heating and cooling has been observed (Ashley et al. 2016). This offset was also detected when calculating entrapment pressure for measurements made at each temperature step. In theory, the calculated entrapment pressure should be identical for each temperature step. However, calculated entrapment pressure exhibited an apparent decrease when the encapsulated inclusions were heated. Independent *P*-*T* estimates are in best agreement with entrapment pressures calculated from measurements obtained when inclusions were heated to the reported formation temperature. There are several factors that may lead to this discrepancy (applying a 1D elastic model for an anisotropic phase, difficulties in accurately modeling quartz volume in proximity of the α- to β-quartz transition, etc.), but regardless the current modeling approach results in entrapment pressure overestimation when using room-*T* measurements in the case of quartz inclusions. In contrast, the heating experiments on apatite inclusions show pressure variations that are in good agreement with the model predictions (Fig. 6). As such, these results suggest that the model

provides good predictions for apatite inclusions within andradite garnet, which suggests that entrapment pressures can be reliably calculated using this approach.

IMPLICATIONS FOR BAROMETRY

Apatite inclusions in garnet can be used for barometry across a wide range of *P*-*T* conditions. Apatite inclusions will be especially useful for rocks in which no other means of pressure estimation is available. Whereas barometry based on chemical equilibrium through net-transfer reactions is common in petrology, numerous environments and systems lack mineral assemblages appropriate for pressure constraints. Certain inclusion minerals are useful petrogenic indicators of formation conditions based solely on phase stability (e.g., coesite, diamond). For minerals such as apatite, which are stable over wide ranges of P and *T*, estimation of retained inclusion pressures based on spectroscopic measurements is a rapidly developing technique in petrologic studies. While apatite-in-garnet has not been used for such applications to date, the extensive stability of apatite in metamorphic and igneous systems, coupled with the ubiquity of apatite in a wide range of rock compositions, make apatite an attractive inclusion mineral to consider for geobarometry. Moreover, apatite exhibits less of a dependence on entrapment temperature than other inclusion-host systems commonly used for barometry (e.g., quartz inclusions in garnet), especially considering chlorapatite inclusions in andradite. Thus, apatite inclusions in garnet permit reasonable pressure estimation even if temperature is only loosely constrained. Heating experiments provide an internal validation that the application of a 1D (isotropic) elastic model is sufficient for calculating entrapment conditions. This is a benefit over using quartz inclusions in garnet because a significant departure between calculated and measured inclusion pressure with heating is observed for quartz, and a correction is needed to

account for the overestimation in entrapment pressures (Ashley et al. 2016). Extensive thermodynamic characterization of mixing in the apatite F-Cl-OH ternary system is still required to better resolve modifications to the elastic parameters in chemically impure crystals. Further research conducting high-resolution *P*-*V*-*T* studies on apatites of different compositions and investigations into *P*- and *T*-induced Raman waveshift may further improve the resolution of this technique.

ACKNOWLEDGEMENTS

We gratefully thank Robert T. Downs and Hexiong Yang for allowing access to the Raman spectroscopy laboratory and for assistance in setting up the heating/freezing stage on the Raman microscope. Review of this manuscript by M. Enami and two anonymous reviewers have greatly improved the clarity of the manuscript.

REFERENCES

Adams, H.G., Cohen, L.H., and Rosenfeld, J.L. (1975) Solid inclusion piezothermometry I: Comparison dilatometry. American Mineralogist, 60, 574-583.

Angel, R.J., Gonzalez-Platas, J., and Alvaro, M. (2014) EosFit7c and a Fortran module (library) for equation of state calculations. Zeitschrift für Kristallographie, 229(5), 405-419.

Antignano, A., and Manning, C.E. (2008) Fluorapatite solubility in H_2O and H_2O–NaCl at 700 to 900 °C and 0.7 to 2.0 GPa. Chemical Geology, 251, 112-119.

Ashley, K.T., Caddick, M.J., Steele-MacInnis, M., Bodnar, R.J., and Dragovic, B. (2014) Geothermobarometric history of subduction recorded by quartz inclusions in garnet. Geochemistry Geophysics Geosystems, 15(2), 350-360.

Ashley, K.T., Darling, R.S., Bodnar, R.J., Law, R.D. (2015) Significance of "stretched" mineral inclusions for reconstructing *P–T* exhumation history. Contributions to Mineralogy and Petrology 169, 55.

Ashley, K.T., Law, R.D., Bodnar, R.J., and Eriksson, K.A. (*accepted*) Quartz inclusions in garnet: Time capsules of early mountain building. In R.D. Law, J.R. Thigpen, H.H. Stowell, A. Merschat, and C. Bailey, Eds. Linkages and Feedbacks in Orogenic Processes, GSA Monograph.

Ashley, K.T., Steele-MacInnis, M., Bodnar, R.J., and Darling, R.S. (2016) Quartz-in-garnet inclusion barometry under fire: Reducing uncertainty from model estimates. Geology, 44, 699-702.

Brunet, F., Allan, D.R., Redfern, S.A.T., Angel, R.J., Miletich, R., Reichmann, H.J., Sergent, J., and Hanfland, M. (1999) Compressibility and tehrmal expansivity of synthetic apatites, $Ca_5(PO_4)_3X$ with X = OH, F and Cl. European Journal of Mineralogy, 11, 1023-1035.

Catlos, E.J., Harrison, T.M., Kohn, M.J., Grove, M., Ryerson, F.J., Manning, C.E., and Upreti, B.N. (2001) Geochronologic and thermobarometric constraints on the evolution of the Main Central Thrust, central Nepal Himalaya. Journal of Geophysical Research-Solid Earth, 106, 16177–16204.

Comodi, P., Liu, Y., and Frezzotti, M.L. (2001) Structural and vibrational behaviour of fluorapatite with pressure. Part II: in situ micro-Raman spectroscopic investigation. Physics and Chemistry of Minerals, 28, 225-231.

Dachs, E., Harlov, D.E., and Benisek, A. (2010) Excess heat capacity and entropy of mixing along the chlorapatite-fluorapatite binary join. Physics and Chemistry of Minerals, 37, 665-676.

Enami, M., Nishiyama, T., and Mouri, T. (2007) Laser Raman microspectrometry of metamorphic quartz: A simple method for comparison of metamorphic pressures. American Mineralogist, 92, 1,303-1,315.

Forien, J.-B., Fleck, C., Krywka, C., Zolotoyabko, E., and Zaslansky, P. (2015) In situ compressibility of carbonated hydroxyapatite in tooth dentine measured under hydrostatic pressure by high energy X-ray diffraction. Journal of the Mechanical Behavior of Biomedical Materials, 50, 171-179.

Gonzalez-Platas, J., Alvaro, M., Nestola, F., and Angel, R.J. (2016) EosFit7-GUI: A new GUI tool for equation of state calculations, analyses and teaching. Journal of Applied Crystallography, 49, 1377-1382.

Guiraud, M., and Powell, R. (2006) *P-V-T* relationships and mineral equilibria in inclusions in minerals. Earth and Planetary Science Letters, 244, 683-694.

Holland, T., and Powell, R. (2011) An improved and extended internally consistent thermodynamic dataset for phases of petrological interest, involving a new equation of state for solids. Journal of Metamorphic Geology, 29, 333-383.

Hovis, G.L., Abraham, T., Hudacek, W., Wildermuth, S., Scott, B., Altomare, C., Medford, A., Conlon, M., Morris, M., Leaman, A., Almer, C., Tomaino, G., and Harlov, D.E. (2015) Thermal expansion of F-Cl apatite crystalline solutions. American Mineralogist, 100, 1040-1046.

Hovis, G.L., and Harlov, D.E. (2010) Solution calormetric investigation of fluor-chlorapatite crystalline solutions. American Mineralogist, 95(7), 946-952.

Hovis, G.L., Scott, B.T., Altomare, C.M., Leaman, A.R., Morris, M.D., Tomaino, G.P., and McCubbin, F.M. (2014) Thermal expansion of fluorapatite-hydroxylapatite crystalline solutions. American Mineralogist, 99, 2171-2175.

Hughes, J.M., Cameron, M., and Crowley, K.D. (1989) Structural variations in natural F, OH, and Cl apatites. American Mineralogist, 74, 870-876.

Konzett, J., and Frost, D.J. (2009) The high P-T stability of hydroxyl-apatite in natural and simplified MORB - an experimental study to 15 GPa with implications for transport and storage of phosphorus and halogens in subduction zones. Journal of Petrology, 50(11), 2043-2062.

Kouketsu, Y., Nishiyama, T., Ikeda, T., Enami, M. (2014) Evaluation of residual pressure in an inclusion–host system using negative frequency shift of quartz Raman spectra. American Mineralogist 99, 433-442.

Liu, J., Glasmacher, U.A., Lang, M., Trautmann, C., Voss, K.-O., Newmann, R., Wagner, G.A., Miletich, R. (2008) Raman spectroscopy of apatite irradiated with swift heavy ions with and without simultaneous exertion of high pressure. Applied Physics A, 91, 17-22.

Liu, X., Shieh, S.R., Fleet, M.E., Zhang, L., and He, Q. (2011) Equation of state of carbonated hydroxylapatite at ambient temperature up to 10 GPa: Significance of carbonate. American Mineralogist, 96, 74-80.

Murayama, J.K., Nakai, S., Kato, M., and Kumazawa, M. (1986) A dense polymorph of $Ca_3(PO_4)_2$: A high pressure phase of apatite decomposition and its geochemical significance. Physics of the Earth and Planetary Interiors, 44, 293-303.

Passchier, C.W., and Trouw, R.A.J. (2005) Microtectonics. 366 p. Springer, Federal Republic of Germany (DEU), Berlin.

Robie, R.A., and Hemingway, B.S. (1995) Thermodynamic properties of minerals and related substances at 298.15 K and 1 bar (10^5 Pascals) pressure and at higher temperatures. United States Geological Survey Bulletin, 2131, 461.

Rosenfeld, J.L., and Chase, A.B. (1961) Pressure and temperature of crystallization from elastic effects around solid inclusions in minerals? American Journal of Science, 259, 519-541.

Schmidt, C., Steele-MacInnis, M., Watenphul, A., and Wilke, M. (2013) Calibration of zircon as a Raman spectroscopic pressure sensor to high temperatures and application to water-silicate melt systems. American Mineralogist, 98, 643-650.

Schmidt, C., and Ziemann, M.A. (2000) In-situ Raman spectroscopy of quartz: A pressure sensor for hydrothermal diamond-anvil cell experiments at elevated temperatures. American Mineralogist, 85, 1725-1734.

Schouwink, P., Miletich, R., Ullrich, A., Glasmacher, U.A., Trautmann, C., Neumann, R., and Kohn, B.P. (2010) Ion tracks in apatite at high pressures: The effect of crytsallographic track orientation on the elastic properties of fluorapatite under hydrostatic compression. Physics and Chemistry of Minerals, 37, 371-387.

Vry, J. K., and Brown, P. E. (1991) Texturally-early fluid inclusions in garnet: Evidence of the prograde metamorphic path? Contributions to Mienralogy and Petrology, 108, 271-282.

Wang, Z., and Ji, S. (2001) Elasticity of six polycrystalline silicate garnets at pressure up to 3.0 GPa. American Mineralogist, 86, 1209-1218.

Watenphul, A., Schmidt, C. (2012) Calibration of berlinite (AlPO4) as Raman spectroscopic pressure sensor for diamond-anvil cell experiments at elevated temperatures. Journal of Raman Spectroscopy, 43, 564-570.

474 Young, E.J., Myers, A.T., Munson, E.L. and Conklin, N.M. (1969) Mineralogy and geochemistry of
475 fluorapatite from Cerro de Mercado, Durango, Mexico. U.S. Geological Survey Professional
476 Paper 650-D, pp. D84-D93.

FIGURE CAPTIONS

Figure 1. Fitted curves from the Tait equation of state of fluorapatite compared to the experimental data of (a) Hovis et al. (2014) and (b) Schouwink et al. (2010).

Figure 2. Isomeke contours for inclusion pressures (in kbar) for apatite inclusions in garnet. Inclusion endmembers include fluorapatite (a,d,g), chlorapatite (b,e,h) and hydroxyapatite (c,f,i). Garnet species modeled as host phase includes almandine (a-c), pyrope (d-f) and andradite (g-i).

Figure 3. (a) Example of peak fitting protocol used in this study, showing the fitted ν_{964} (phosphate symmetric stretch) and ν_{950} (radiation damage) peaks. The lower wavenumber tail of the ν_{1030} (phosphate antisymmetric stretch) peak is visible on the right hand side. See text for additional details. (b) The ν_{964} Raman band of Durango fluorapatite, as a function of temperature. Spectra in black were acquired along the heating path, whereas spectra in dashed gray lines were acquired along the cooling path.

Figure 4. Pressure-sensitive Raman waveshift regression for fluorapatite calculated from the experimental data of Schouwink et al. (2010). The polynomial expression can be used to calculate inclusion pressures for fully encapsulated apatite inclusions and formation pressure can be determined using the isomeke contours in Figure 2.

499 **Figure 5.** Temperature-sensitive Raman waveshift regression for Durango (fluor)apatite and
500 apatite from the Casting Copper mine, Yerington district, NV.
501
502 **Figure 6.** Inclusion pressures of the Casting Copper apatite inclusions as a function of
503 temperature. The line shows the predicted P_{incl}-T relationship, calculated with the 1D
504 elastic model.
505
506

This is a preprint, the final version is subject to change, of the American Mineralogist (MSA)
Cite as Authors (Year) Title. American Mineralogist, in press.
(DOI will not work until issue is live.) DOI: http://dx.doi.org/10.2138/am-2017-5898

Figure 1

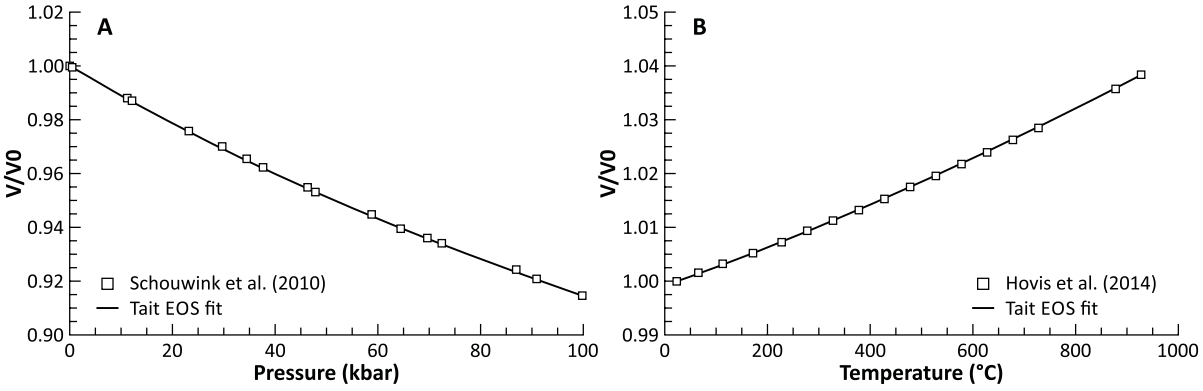

This is a preprint, the final version is subject to change, of the American Mineralogist (MSA)
Cite as Authors (Year) Title. American Mineralogist, in press.
(DOI will not work until issue is live.) DOI: http://dx.doi.org/10.2138/am-2017-5898

Figure 2

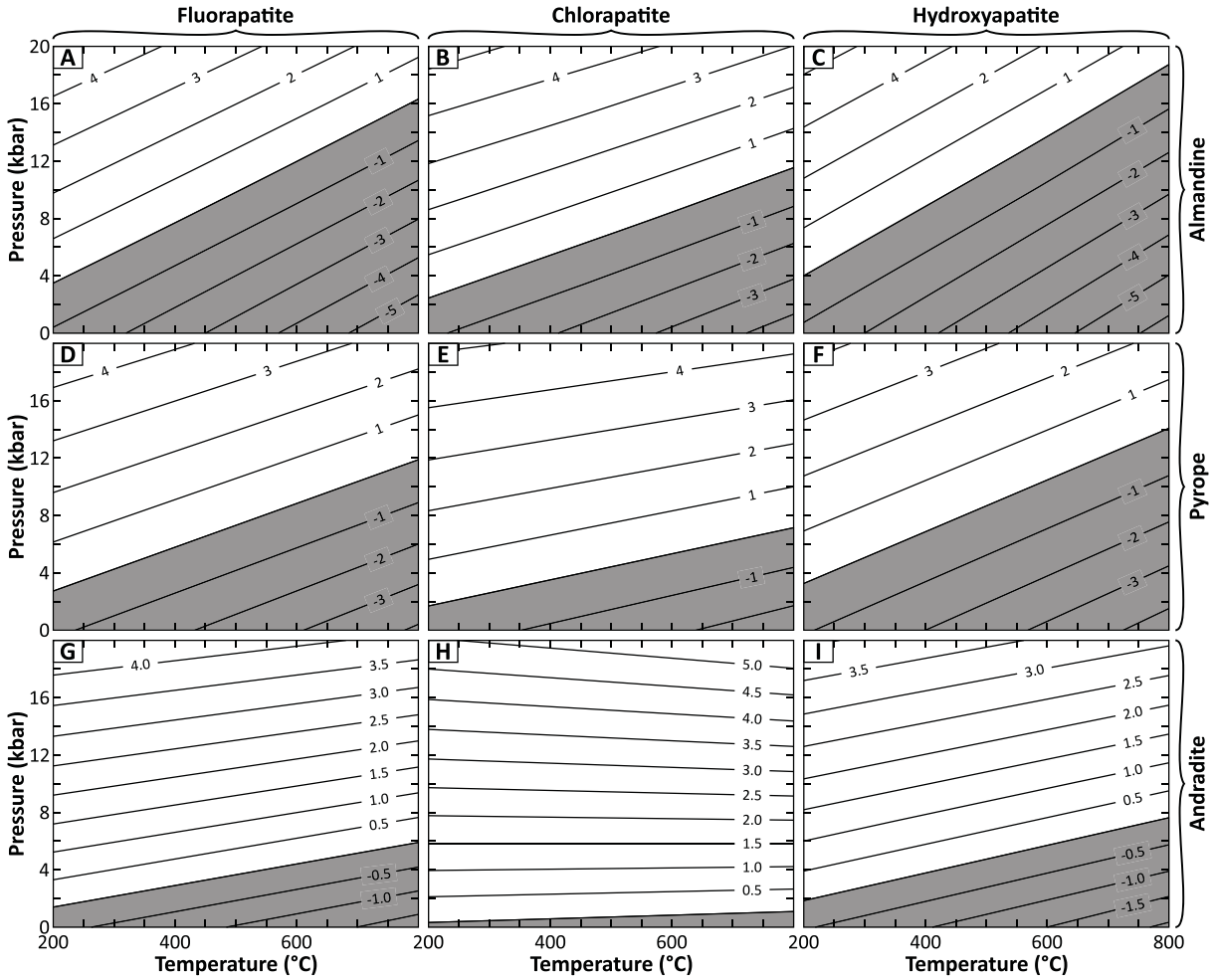

This is a preprint, the final version is subject to change, of the American Mineralogist (MSA)
Cite as Authors (Year) Title. American Mineralogist, in press.
(DOI will not work until issue is live.) DOI: http://dx.doi.org/10.2138/am-2017-5898

Figure 3

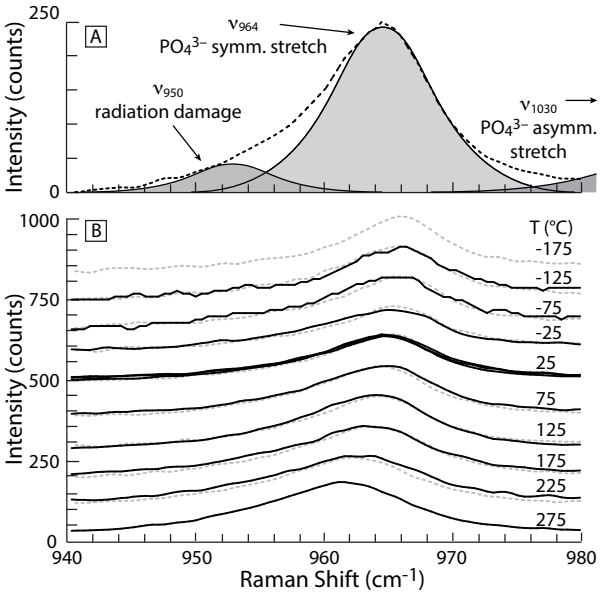

This is a preprint, the final version is subject to change, of the American Mineralogist (MSA)
Cite as Authors (Year) Title. American Mineralogist, in press.
(DOI will not work until issue is live.) DOI: http://dx.doi.org/10.2138/am-2017-5898

Figure 4

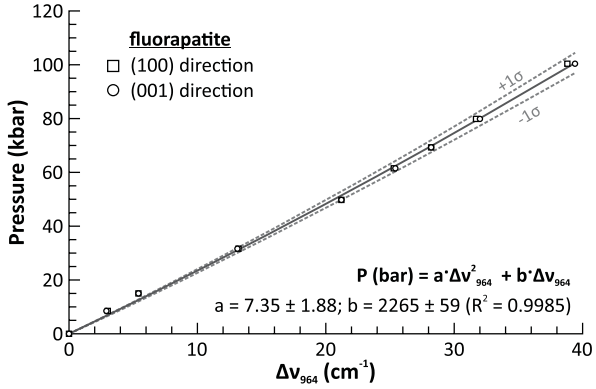

This is a preprint, the final version is subject to change, of the American Mineralogist (MSA)
Cite as Authors (Year) Title. American Mineralogist, in press.
(DOI will not work until issue is live.) DOI: http://dx.doi.org/10.2138/am-2017-5898

Figure 5

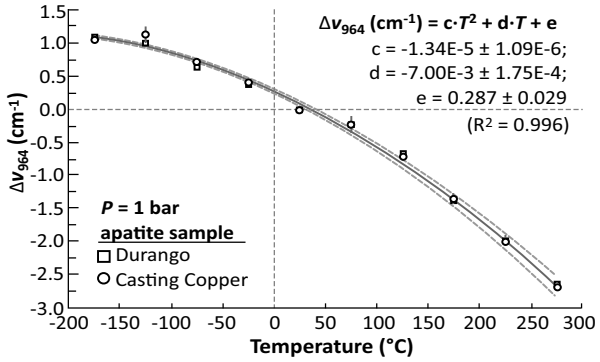

This is a preprint, the final version is subject to change, of the American Mineralogist (MSA)
Cite as Authors (Year) Title. American Mineralogist, in press.
(DOI will not work until issue is live.) DOI: http://dx.doi.org/10.2138/am-2017-5898

Figure 6

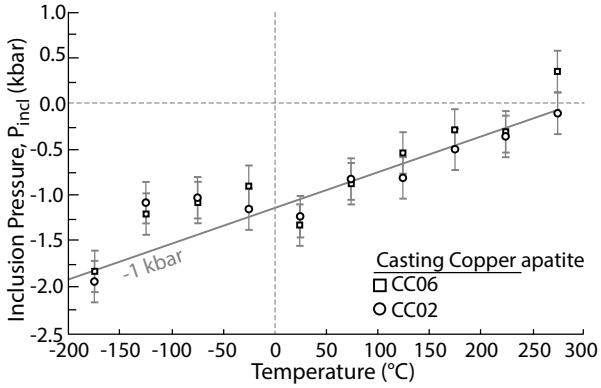

This is a preprint, the final version is subject to change, of the American Mineralogist (MSA)
Cite as Authors (Year) Title. American Mineralogist, in press.
(DOI will not work until issue is live.) DOI: http://dx.doi.org/10.2138/am-2017-5898

Table 1. Sources of volume data used for EOS fitting of apatite endmembers

	Thermal Expansion	**Compressibility**
fluorapatite	Hovis et al. (2014) – *Durango, Mexico*	Schouwink et al. (2010) – *Durango, Mexico*
chlorapatite	Hovis et al. (2015) – *APS26 (synthetic)*	Brunet et al. (1999) – synthetic
hydroxyapatite	Hovis et al. (2014) – *Holly Springs, Georgia*	Brunet et al. (1999) – synthetic

Note: Sample localities are given for natural samples. Please see respective sources for additional information, including apatite chemistry.

This is a preprint, the final version is subject to change, of the American Mineralogist (MSA)
Cite as Authors (Year) Title. American Mineralogist, in press.
(DOI will not work until issue is live.) DOI: http://dx.doi.org/10.2138/am-2017-5898

Table 2. Thermodynamic properties and modified Tait *P-V-T* EOS fit parameters of apatite

	$S°_{298}$ (J mol^{-1} K^{-1})	V_{298} (Å^3)	α_{298} x 10^6 (K^{-1})	κ_{298} (kbar)	κ'_{298}	κ''_{298} (kbar^{-1})	θ_E (K)
Fl-apatite	383.2(1.5)[1]	525.86(3)	32.9(3)	868(5)	5.63(15)	-0.00648	430.82
Cl-apatite	400.6(1.6)[1]	544.86(11)	30.0(2.5)	846(58)	6.6(1.0)	-0.00779	416.83
OH-apatite	390.4(1.7)[2]	529.32(3)	33.6(7)	913(15)	5.55(26)	-0.00608	424.92

Note: κ''_{298} is an estimated value from the EOS fitting and the Einstein temperature (θ_E) is estimated by $\theta_E = 10636/(S°_{298}/n_i + 6.44)$, where n_i is the number of atoms in the endmember *i* (see Holland and Powell 2011 for details).

[1]Dachs et al. (2010); [2]Robie and Hemingway (1995)

This is a preprint, the final version is subject to change, of the American Mineralogist (MSA)
Cite as Authors (Year) Title. American Mineralogist, in press.
(DOI will not work until issue is live.) DOI: http://dx.doi.org/10.2138/am-2017-5898

Table 3. Raman spectroscopic heating data on apatite samples

T	Durango[1]	CC01[2]	CCO2[3]			CC06[3]		
(°C)	ν_{964}	ν_{964}	ν_{964}	$\Delta\nu_{964}$[4]	P (bar)	ν_{964}	$\Delta\nu_{964}$[4]	P (bar)
25	965.32	966.24	965.76	-0.51	-1380	965.76	-0.51	-1380
75	965.17	966.08	965.51	-0.76	-1003	965.62	-0.65	-754
125	964.63	965.53	965.23	-1.04	-542	965.13	-1.14	-768
175	963.90	964.85	964.76	-1.51	-358	964.67	-1.60	-562
225	963.31	964.22	964.04	-2.23	-589	963.99	-2.28	-702
275	962.68	963.58	963.77	-2.50	351	963.57	-2.70	-103
225	963.37	964.32	964.29	-1.98	-23	964.29	-1.98	-23
175	963.96	964.96	964.82	-1.45	-223	964.72	-1.55	-449
125	964.70	965.60	965.24	-1.03	-519	965.10	-1.17	-835
75	965.00	966.02	965.63	-0.64	-731	965.56	-0.71	-890
25	965.33	966.32	965.71	-0.56	-1492	965.83	-0.44	-1222
-25	965.71	966.65	966.26	-0.01	-1041	966.29	0.02	-973
-75	965.99	966.98	966.43	0.16	-1296	966.65	0.38	-799
-125	966.37	967.33	966.70	0.43	-1174	966.73	0.46	-1106
-175	966.42	967.33	966.56	0.29	-1826	966.51	0.24	-1939
-125	966.30	967.48	966.68	0.41	-1219	966.75	0.48	-1061
-75	965.92	966.96	966.62	0.35	-867	966.44	0.17	-1274
-25	965.67	966.68	966.39	0.12	-747	966.13	-0.14	-1334
25	965.31	966.24	965.89	-0.38	-1086	965.89	-0.38	-1086

[1]Fluorapatite standard from Durango (Cerro de Mercado mine), Mexico
[2]Fluorapatite inclusion in garnet from the Casting Copper mine, Yerington district, NV. Exposed at the sample surface.
[3]Fluorapatite inclusion in garnet from the Casting Copper mine, Yerington district, NV. Fully encapsulated within garnet.
[4]Waveshifts relative to average ν_{964} for CC01 at 25 °C and 1 bar (966.27 ± 0.05 cm^{-1})